Effects of Temperature on the Crystal and Molecular Structure of the Mixed-Valence Linear Chain $[Pt(en)_2][Pt(en)_2X_2](ClO_4)_4$ (X = Cl, Br)

Sara C. Huckett, Brian Scott, Steven P. Love, Robert J. Donohoe, Carol J. Burns, Ed Garcia, Tracey Frankcom, and Basil I. Swanson*

Spectroscopy and Biochemistry Group (INC-14), Los Alamos National Laboratory, Los Alamos, New Mexico 87544

Received June 22, 1992

The crystal structures of the pure monoclinic and orthorhombic phases of $[Pt(en)_2][Pt(en)_2Cl_2](ClO_4)_4$ (PtCl) and $[Pt(en)_2][Pt(en)_2Br_2](ClO_4)_4$ (PtBr), with en = 1,2-diaminoethane, were determined at several temperatures. The monoclinic phase of PtCl has space group $P2_1/m$, with a = 7.972(3) Å, b = 10.874(5) Å, c = 8.500(4) Å, β = 108.91(4)°, Z = 2, d = 2.619 g/cm^3, and T = −20 °C. The monoclinic phase of PtBr crystallizes in space group $P2_1/m$, with a = 7.959(2) Å, b = 10.957(2) Å, c = 8.529(2) Å, β = 109.32(3)°, Z = 2, d = 2.811 g/cm^3, and T = 25 °C. The orthorhombic phase of PtCl has space group *Ibam*, with a = 13.594(4) Å, b = 9.657(5) Å, c = 10.855(4) Å, Z = 4, d = 2.562 g/cm^3, and T = 25 °C. The orthorhombic phase of PtBr crystallizes in space group *Ibam*, with a = 13.671(5) Å, b = 9.680(3) Å, c = 10.994(3) Å, Z = 4, d = 2.712 g/cm^3, and T = 40 °C. The monoclinic phases of PtCl and PtBr were also determined at T = −70 and −93 °C, respectively. The lattice constants for PtCl(−70 °C) are a = 7.947(4) Å, b = 10.871(5) Å, c = 8.445(5) Å, and β = 108.79(4)°, and the lattice constants for PtBr(−93 °C) are a = 7.912(2) Å, b = 10.900(2) Å, c = 8.387(2) Å, and β = 109.02(3)°. The corresponding PtCl and PtBr phases are isostructural. These systems contain chains composed of alternating, octahedral $Pt(en)_2X_2$ and square planar (4 + 2) $Pt(en)_2$ species; the axial halides of the octahedral species occupy semicoordinate axial sites of the square planar species. This motif results in alternating Pt–X distances along the chain, resulting in a charge density wave (CDW). The chains are linked together via a weak hydrogen-bonding network involving the NH_2 hydrogens of the ethylenediamine ligands and the perchlorate counterions. The major structural differences between the phases are related to changes in the hydrogen bonding brought on by increased thermal motions of the perchlorate ions as the temperature is raised. These changes in hydrogen bonding alter crystal packing and incur subtle changes in PtX chain geometry and CDW strength. Raman spectroscopy measurements show a direct correlation between the frequency of the fundamental X–Pt–X stretch and the strength of the CDW.

Introduction

MX systems are comprised of one-dimensional chains of alternating metal and halide centers.[1] These materials have the general stoichiometry $[M(L\text{-}L)_2][M(L\text{-}L)_2X_2]Y_4$, where M = Pt, Pd, and Ni, L-L = ethylenediamine, propylenediamine, and cyclohexylenediamine, and Y = X^-, ClO_4^-, and BF_4^-. The L-L ligands bond to the Pt atoms, defining an equatorial plane perpendicular to the chain axis. The Y anions serve to link the chains together via a weak hydrogen-bonding network. These systems are susceptible to a Peierls distortion and charge disproportionation, producing a dimerization of the halogen sublattice and alternating valence states on the metals along the chain axis: X–Pt(IV)–X···Pt(II)···X. The strength of this CDW, which may be measured experimentally as ρ = M(IV)–X/M(II)···X, may be tuned by altering the bridging halide, the equatorial amine ligands, metal atom, and counterion.[1b] A recent study by this group (vide infra) on a series of PtX materials has also mapped out relationships between ρ, symmetric X–Pt–X stretching frequency (ν_1), and the intervalence charge-transfer energy.

These materials exhibit anisotropic electronic and optical properties which have been the subject of numerous investigations over the last two decades.[1] In recent years, this group has focused on the system $[Pt(en)_2][Pt(en)_2X_2](ClO_4)_4$ (X = Cl, Br, I; PtCl, PtBr, and PtI, respectively) in order to gain an in depth understanding of these materials. In order to help explain the observed properties and learn more about the underlying electron–phonon interactions at work in these materials, techniques including resonance Raman[2] and EPR[3] spectroscopies and scanning tunneling microscopy (STM)[4] have been employed. Theoretical modeling of these systems is also an area of current interest.[5] A viable theoretical model not only aids in understanding MX solids but holds hopes of being applied to more complex systems.[6]

Structural characterization of MX compounds has been important in its own right, but also in conjunction with the techniques discussed above. Correlations between structure and

(1) (a) Keller, H. J. In *Extended Linear Chain Compounds*; Miller, J. S., Ed.; Plenum Press: New York, 1982; Vol. 3. (b) Clark, R. J. H.; Croud, V. B.; Wills, R. J.; Bates, P. A.; Dawes, H. M.; Hursthouse, M. B. *Acta Crystallogr.* **1989**, *B45*, 147.

(2) (a) Tanaka, M.; Kurita, S. *J. Phys. C* **1986**, *19*, 3019. (b) Clark, R. J. H.; Croud, V. B. In *Organic and Inorganic Low-Dimensional Crystalline Materials*; Delhaes, P., Drillon, M. Eds.; Plenum: New York, 1987. (c) Conradson, S. D.; Dallinger, R. F.; Swanson, B. I.; Clark, R. J. H.; Croud, V. B. *Chem. Phys. Lett.* **1987**, *135*, 463. (d) Donohoe, T. J.; Ekberg, S. A.; Tait, C. D.; Swanson, B. I. *Solid State Commun.* **1989**, *71*, 49. (e) Fanizzi, F. P.; Natile, G.; Tiripicchio, A.; Clark, R. J. H.; Michael, D. J. *J. Chem. Soc., Dalton Trans.* **1989**, 1689. (f) Donohoe, R. J.; Dyer, R. B.; Swanson, B. I. *Solid State Commun.* **1990**, *73*, 521. (g) Donohoe, R. J.; Tait, C. D.; Swanson, B. I. *Chem. Mater.* **1990**, *2*, 315.

(3) (a) Kawamori, A.; Aoki, R.; Yamashita, M. *J. Phys. C: Solid State Phys.* **1985**, *18*, 5487. (b) Kurita, S.; Haruki, M. *Synth. Met.* **1989**, *29*, F129. (c) Haruki, M.; Kurita, S. *Phys. Rev. B* **1989**, *39*, 5706.

(4) (a) Weinrach, J. B.; Hawley, M.; Sattelberger, A. P.; Swanson, B. I. *Solid State Commun.* **1991**, *77*, 853. (b) Donohoe, R. J.; Worl, L. A.; Arrington, C. A.; Bulou, A.; Swanson, B. I. *Phys. Rev. B* **1992**, *45*, 185.

(5) (a) Ueta, M.; Kanzaki, H.; Kobayashi, K.; Toyazawa, Y.; Hanamura, E. In *Excitonic Processes in Solids*; Springer Ser. Solid State Sci. 60; Springer: New York, 1986. (b) Onodera, Y. *J. Phys. Soc. Jpn.* **1987**, *56*, 250. (c) Baeriswyl, D.; Bishop, A. R. *J. Phys. C: Solid State Phys.* **1988**, *21*, 339. (d) Nasu, K.; Mishima, A. *Rev. Solid-State Sci.* **1988**, *2*, 539. (e) Mishima, A.; Nasu, K. *Phys. Rev. B* **1989**, *39*, 5758. (f) Mishima, A.; Nasu, K. *Phys. Rev. B* **1989**, *39*, 5763.

(6) Baeriswyl, D.; Bishop, A. R. *Phys. Scr.* **1987**, *T19*, 239.

0020-1669/93/1332-2137$04.00/0

conductivity have been made.[7] In addition, atomic force microscopy (AFM) and scanning tunneling microscopy (STM) results coupled with known X-ray data should provide information concerning long-range structure and local structure of defects including polarons, bipolarons, excitons, and kinks.[4] Accurate structural parameters such as bond distances and angles are clearly required for theoretical approaches such as lattice dynamics[8] and many-body modeling.[9]

This group has recently grown a range of quality mixed-halide crystals of stoichiometry $PtCl_{1-y}I_y$ and $PtBr_{1-y}I_y$ (y = 0.0–0.4 or 1.0–0.6). Many-body theoretical calculations[10a] predict partial charge separation across the junctions in these systems, with charge being injected from PtI segments into PtX segments. Preliminary X-ray diffraction and resonance Raman spectroscopy support such a picture.[10b] The superstructure, or segment distribution, in these systems is presently being investigated using real imaging techniques such as AFM. However, since PtBr and PtCl serve as host lattices in these materials, it is essential to know the structures of these materials at a very detailed and correct level. Ultimately, it is hoped that the revealed superstructure can be synthetically controlled, opening the door to a new class of nanostructural materials.

This laboratory has also investigated the photoinduced charge separation in photoexcited single crystals of $PtCl_xBr_{1-x}$ (x = 0.0–1.0) mixed-halide crystals.[10c,d] Resonance Raman studies clearly indicated charge separation, with electron polarons locating on PtBr segments and hole polarons on PtCl segments. Such systems have potential applications as photovoltaic and photoconductive devices. Again, fabrication of these devices relies on an understanding of segment distribution. AFM studies are in progress in order to determine segment distribution. A clear understanding of the structures of the pure materials is essential to this effort.

Structural characterization of the MX materials has proven surprisingly complex. Four different crystal structures of PtBr have been reported.[11] Two orthorhombic structures, with identical lattice parameters, have been reported in space groups $I222$[11b] and $Ic2a$ ($Ibam$).[11a] Two monoclinic structures, with identical lattice parameters, have been reported in space groups $P2$[11a] and $P2_1/m$.[11c] Additionally, a PtBr crystal was shown to undergo a monoclinic to orthorhombic phase transformation under Cu Kα irradiation.[11a] With respect to resonance Raman experiments PtBr had previously proven problematic in that the ν_1 band components, which in principle could be attributed to factor group splittings, were inconsistent[2c] with the published crystal structure.[11b] The sample dependence observed for both PtBr resonance Raman ν_1 fine structure[2] and single-crystal diffraction experiments[11] has now been shown to result from chloride ion impurities.[12] In addition, differential scanning calorimetry (DSC) demonstrates that both PtBr and PtCl undergo a monoclinic to orthorhombic phase change around room temperature (28.7 and 19.8 °C, respectively).[12a] A recent neutron powder diffraction study of the phase transition in PtCl has also been reported.[12b] A recent study by Toriumi et al.[11c] on the pure orthorhombic PtBr phase was carried out at 25 °C, a temperature approximately 4 °C below the PtBr phase transition. Such a determination raises questions regarding phase inhomogeneity of the orthorhombic crystals. The structure of PtCl has previously been determined only in the high-temperature (>20 °C) orthorhombic phase.[13]

In view of these complexities, and the importance of obtaining reliable structural information for pure PtX systems, the single-crystal X-ray diffraction characterizations of the pure orthorhombic and monoclinic phases of PtBr and PtCl were performed. Low-temperature structures were performed on the monoclinic phases of PtCl and PtBr. The following issues will be addressed in this work:

(1) It will be demonstrated that only one unique space group exists for each of the orthorhombic and monoclinic phases of PtBr and PtCl. The errors in previous space group assignments will be discussed in light of Cl impurities. (2) The monoclinic phase of PtCl will be determined for the first time. The orthorhombic phase structure determination is compared with the structure of Kida et al.,[13] where anomalous lattice constants have been noted. The most suspect lattice constant corresponds to the chain axis and is quite short. (3) The structure of the orthorhombic phase of PtBr was determined at 40 °C, well above the monoclinic to orthorhombic phase transition. The structure of the corresponding monoclinic phase was determined at 25 °C, which is several degrees below the PtBr phase transition. Such structures will be void of any phase inhomogeneities. (4) The temperature dependence of the CDW will be mapped out. This is an important relationship in the design of advanced materials. The X-ray diffraction and resonance Raman results will be employed to define this dependence.

Experimental Section

Sample Preparation. PtCl[14] and PtBr(25 °C)[12] were prepared according to literature methods from $Pt(en)_2Cl_2$ and $Pt(en)_2(ClO_4)_2$, respectively. PtBr (25 °C) was recrystallized from a large crystal shown by ^1H NMR to contain <2% Cl.[12a] PtBr(40 °C) was prepared by dissolving equimolar amounts of $Pt(en)_2Br_2$ and $Pt(en)_2Br_4$ in a dilute perchloric acid solution. ($Pt(en)_2Br_2$ was prepared from K_2PtBr_4 and 1,2-diaminoethane. $Pt(en)_2Br_4$ was made by oxidizing $Pt(en)_2Br_2$ with bromine.) Except where otherwise noted, all materials were recrystallized from H_2O at ~10 °C by placing a beaker of the compound dissolved in water into a closed container containing $MgSO_4$. PtBr formed metallic green needle-shaped crystals, while PtCl formed red needle-shaped crystals.

Warning: *Perchlorate salts are potentially explosive and should be handled with great caution!*[15]

X-ray Diffraction. All crystals were mounted on thin glass fibers, and data collection was carried out on either a fully automated Siemans R3m/v or Enraf Nonius CAD4 diffractometer. The PtCl crystals used for the low-temperature (monoclinic) determinations at –20 and –70 °C were mounted in a cold room at 4 °C and kept on the goniometer head in a dewar with dry ice before quickly transferring to the diffractometer under a liquid-N_2 stream of the appropriate temperature. The PtCl orthorhombic phase was determined at 25 °C. The PtBr crystal used for the high-temperature (orthorhombic) determination was heated to 40 °C on the diffractometer using a heated stream of dry air. The structures of the monoclinic phases of PtBr were carried out at room temperature (25 °C) and –93 °C. Graphite-monochromatized Mo Kα radiation (λ = 0.710 69 Å) was employed on both instruments. The orientation matrix and lattice parameters were optimized from a least-squares calculation on at least 25 carefully centered reflections with high Bragg angles. At least 2 standard reflections were monitored every 96 reflections and showed no systematic variation. Extended axial photographs (>1 h) of all samples

(7) Allen, S. D.; Clark, R. J. H.; Croud, V. B.; Kurmoo, M. *Phil. Trans. R. Soc. London A* **1985**, *314*, 131.
(8) (a) Bulou, A.; Donohoe, R. J.; Swanson, B. I. *J. Phys.: Condensed Matter* **1991**, *3*, 1709. (b) Bulou, A.; Donohoe, R. J.; Swanson, B. I. *Phys. Rev. B* **1990**, *42*, 10566.
(9) (a) Bishop, A. R.; Gammel, J. T. *Synth. Met.* **1989**, *29*, F151. (b) Gammel, J. T.; Donohoe, R. J.; Bishop, A. R.; Swanson, B. I. *Phys. Rev. B* **1990**, *42*, 10566.
(10) (a) Saxena, A.; Bishop, A. R.; Worl, L. A.; Swanson, B. I. *Synth. Met.* **1992**, *51*, 431. (b) Scott, B.; Johnson, S. R.; Swanson, B. I. *Synth. Met.*, in press. (c) Worl, L. A.; Huckett, S. C.; Swanson, B. I.; Saxena, A.; Bishop, A. R.; Gammel, J. T. *J. Phys. C* **1992**, *4*, 10237. (d) Huang, X. Z.; Saxena, A.; Bishop, A. R.; Worl, L. A.; Love, S. P.; Swanson, B. I. *Solid State Commun.* **1992**, *84*, 951.
(11) (a) Keller, H. J.; Muller, B.; Ledezma, G.; Martin, R. *Acta Crystallogr.* **1985**, *C41*, 16. (b) Endres, H.; Keller, H. J.; Martin, R.; Traeger, U.; Novotny, M. *Acta Crystallogr.* **1980**, *B36*, 35. (c) Toriumi, K.; Yamashita, M.; Kurita, S.; MuraseI.; Ito, T. *Acta Crystallogr. B*, in press.
(12) (a) Huckett, S. C.; Donohoe, R. J.; Worl, L. A.; Bulou, A. D. F.; Burns, C. J.; Laia, J. R.; Carroll, D.; Swanson, B. I. *Chem. Mater.* **1991**, *3*, 123. (b) Bulou, A.; Huckett, S.; Garcia, E.; Swanson, B. I.; Kwei, G. H.; Eckert, J. *Ferroelectrics* **1992**, *125*, 3550.
(13) Matsumoto, N.; Yamashita, M.; Ueda, I.; Kida, S. *Mem. Fac. Sci., Kyushu Univ. Ser. C* **1978**, *11*, 209.
(14) Bekaroglu, O.; Breer, H.; Endres, H.; Keller, H. J.; Nam Gung, H. *Inorg. Chim. Acta* **1977**, *21*, 183.
(15) (a) *J. Chem. Educ.* **1973**, *50*, A335. (b) *Chem. Eng. News* **1983**, *61* (Dec 5), 4.

Table I. Crystalographic Data for the Chloride and Bromide Structures

(a) $[Pt(C_2H_8N_2)_2Cl_2][Pt(C_2H_8N_2)_2](ClO_4)_4$ Structures

	T/°C		
	25	−20	−70
fw	1099.3	1099.3	1099.3
space group	*Ibam* (No. 72)	$P2_1/m$ (No. 11)	$P2_1/m$ (No. 11)
a/Å	13.594(4)	7.972(3)	7.947(4)
b/Å	9.657(5)	10.874(5)	10.871(5)
c/Å	10.855(4)	8.500(4)	8.445(5)
β/deg		108.81(4)	108.79(4)
V/Å^3	1424.9(9)	697.1(5)	690.7
Z	4	2	2
d_x (g/cm^3)	2.562	2.619	2.643
μ/cm^{-1}	106	107	108
λ(Mo Kα)/Å	0.710 69	0.710 69	0.710 69
R^a	0.0192	0.0286	0.0221
$R_w{}^b$	0.0267	0.0403	0.0350

(b) $[Pt(C_2H_8N_2)_2Br_2][Pt(C_2H_8N_2)_2](ClO_4)_4$ Structures

	T/°C		
	40	25	−93
fw	1188.2	1188.2	1188.2
space group	*Ibam* (No. 72)	$P2_1/m$ (No. 11)	$P2_1/m$ (No. 11)
a/Å	13.671(5)	7.959(2)	7.912(2)
b/Å	9.680(3)	10.957(2)	10.900(2)
c/Å	10.994(3)	8.529(2)	8.387(2)
β/deg		109.31(3)	109.02(3)
V/Å^3	1454.8(8)	697.1(5)	683.8(3)
Z	4	2	2
d_x (g/cm^3)	2.712	2811	2.885
μ/cm^{-1}	129	133	137
λ(Mo Kα)/Å	0.710 69	0.710 69	0.710 69
R^a	0.0298	0.0206	0.0204
$R_w{}^b$	0.0258	0.0281	0.0288

^{a} $R = \sum\|F_o| - |F_c\|/\sum|F_o|$. ^{b} $R_w = [\sum(w^{1/2}(|F_o| - |F_c|)/\sum w^{1/2}|F_o|]$.

showed diffuse sheets corresponding to one-half the chain axis dimension. All data reductions, including Lorentz and polarization corrections, structure solution and refinement, and graphics, were performed using SHELXTL PLUS[16] software. Scattering factors were taken from ref 17. The quantity minimized was $\sum_w(F_o - F_c)$, where $w^{-1} = s^2(F) + (g)F^2$ and g was chosen to give the least variation of the mean value of $w(F_o - F_c)^2$ as a function of the magnitude of F_o. All data sets were corrected for absorption using an emperical method.[18] Experimental details of single-crystal X-ray diffraction data collection and handling are reported in Table I.

PtBr (25 and −93 °C). Systematic absences were observed for only $0k0$ reflections. Of the six reflections in this class where $k = 2n + 1$ all six are unobserved. The previously published monoclinic PtBr structure by Keller et al. does not confirm these absences.[11b] However, the absences observed in the recent work by Toriumi et al. is in agreement with ours.[11c] These absences indicate a 2_1 screw axis, leading to the possible space groups $P2_1$ and $P2_1/m$. The latter was chosen since statistical analysis of the data indicated a centrosymmetric space group. Later attempts at refinement in acentric space groups $P2_1$, $P2$, and Pm failed. Attempts at refinement in the centric space group $P2/m$ also failed.

Refinement of the structure was initiated by placing Pt at the origin and the bridging Br at 0, $^1/_4$, 0 (by analogy to the literature structure[11a]) and holding their positions fixed. The Cl atoms of the perchlorate anions were located from a difference Fourier, whereupon the bridging Br was moved slightly off the mirror plane at $y = {}^1/_4$, its site occupancy parameter held at 0.5, and the y positional parameter allowed to vary. At this point the refinement proceeded smoothly via difference Fourier and least-squares techniques to locate and refine the positional parameters of the remaining non-hydrogen atoms. The final refinement cycle included anisotropic thermal parameters for all non-hydrogen atoms. The H atom distances were fixed at C–H = 0.96 Å and N–H = 0.90 Å, with isotropic thermal parameters fixed at 0.08 Å^2.

PtBr (40 °C). Systematic absences that correspond to space groups *Ic2a* and *Icma* were observed. However, a centrosymmetric cell was strongly indicated by the data, and contrary to the results of Keller et al.,[11a] *Icma* was chosen for refinement. (Attempts to refine the structure in the acentric space group *Ic2a* were unsuccesful.) The cell parameters were transformed to correspond to the standard space group *Ibam*. Data were corrected for absorption using an empirical method. Once again refinement was initiated by the placement of Pt and Br in the unit cell by analogy to previous structural work.[11a] In this case the Pt was located at 0, 0, $^1/_4$, and the bromine, at the origin. The Cl was located from a difference Fourier and allowed to refine along with the Br that moved slightly off the mirror plane at the origin. The location and refinement of the C and N atoms was straightforward and was accomplished by standard difference Fourier and least-squares techniques. The oxygens of the perchlorate anion were somewhat more problematical in that some disorder was encountered. The two oxygen atoms that are located a $z = {}^1/_2$ (i.e. coplanar with the Cl on the mirror plane) are split between two positions giving a total of four oxygen positions with $^1/_4$ occupancy. The oxygens located above and below the mirror plane do not exhibit any disorder. The hydrogen atoms were treated as in PtBr(25 °C). The final refinement included anisotropic thermal parameters on all non-hydrogen atoms.

PtCl (−20 and −70 °C). Systematic absences and statistical analysis, in a fashion analagous to PtBr(25 °C), indicated assignment of $P2_1/m$ as the space group. Refinement of the structure was initiated by placement of the Pt atom at 0, 0, 0. The Cl, N, C, and O atoms were located and refined as for PtBr(25 °C). All non-hydrogen atoms were refined anisotropically. H atoms were treated as in PtBr(25 °C).

PtCl (25 °C). Systematic absences and statistical analysis resulted in the assignment of the space group *Ibam*. The Pt was fixed at 0, 0, $^1/_4$. The bridging Cl was located from the difference Fourier and placed at 0, 0, 0.47. The remaining atoms were located from subsequent difference Fouriers, and standard least-squares techniques were used to refine the positional parameters. A disorder of the O atoms on the $z = {}^1/_2$ mirror plane was modeled by placing four oxygen atoms on the mirror plane and fixing their site occupancy factors at $^1/_4$. The final refinement cycles included anisotropic thermal parameters for all non-hydrogen atoms. H atoms were treated as described above.

Raman Measurements. All measurements were performed in the back-scattering geometry, with the laser light polarized parallel to the chain axis, using a Spex Model 1877D triple spectrograph equipped with a Princeton Instruments 298 × 1152 element charge-coupled device (CCD) array detector. Excitation in the 700–980-nm range was provided by a Spectra-Physics Model 3900 Ti:sapphire laser pumped by an Ar^+ ion laser; measurements using the 514.5-nm line of the Ar^+ laser were also performed. Single-crystal samples were mounted on a copper block attached to the cold stage of an Air Products Displex closed-cycle helium refrigerator, and the sample temperature was monitored using both a thermocouple and a diode thermometer mounted near the sample position with silicone heat-sink grease. To avoid laser heating of the sample, laser power at the sample was kept below 0.2 mW, focused to an approximately 0.3-mm-diameter spot. The spectrograph was set up to allow a small amount of elastically scattered laser light to fall on the CCD array at the same time as the Raman scattered light. This permits the laser wavelength to be known at all times, eliminating the ambiguity which otherwise can arise from small wavelength shifts of the Ti:sapphire laser during the course of an experiment.

For PtCl, crystals grown and maintained in both the high- and low-temperature phases were studied. Separate Raman experiments monitored the effects of both cooling the orthorhombic crystals and warming the monoclinic crystals through the phase transition. Experiments were performed on both ordinary PtCl with natural Cl isotopic abundance and on isotopically enriched samples with roughly 99% pure ^{35}Cl on the chains. For PtBr, crystals were grown in the monoclinic phase at 20 °C, and measurements were first made down to 15 K before warming through the phase transition.

Structure Description

The orthorhombic phases of PtCl and PtBr are isostructural, as are their monoclinic phases. The orthorhombic phases crystallize in the space group Ibam, the monoclinic phases in $P2_1/m$. The structure description will deal with the Ibam and $P2_1/m$ structures in turn. The Ibam structures include PtBr(40 °C) and PtCl(25 °C). The $P2_1/m$ structures are PtCl(−20 °C), PtCl(−70 °C), PtBr(25 °C), and PtBr(−93 °C). The atomic

(16) Sheldrick, G. M. SHEXTL PLUS. Siemans Analytical X-Ray Instruments, Madison, WI, 1990.
(17) (a) Cromer, D. T.; Waber, J. T. *International Tables for X-ray Crysallography*; Kynoch Press: Birmingham, England; 1974; Table 2.3.1. (b) Cromer, D. T. *Ibid.*, Table 2.3.1.
(18) Walker, N.; Stuart, D. *Acta Crystallogr.* **1983**, *A39*, 158.

Table II. Atomic Positions ($\times 10^4$ Å) and Isotropic Thermal Parameters (Å$^2 \times 10^3$) for the Title Compounds

atom	x	y	z	U(eq)[a]
		PtBr(40 °C)		
Pt	0	0	2500	25(1)
Br	0	0	237(2)	36(1)
Cl	2992(3)	776(4)	5000	52(1)
N(1)	1003(4)	1591(6)	2527(13)	44(2)
C(1)	479(7)	2918(10)	2796(9)	59(4)
O(1)	2617(7)	164(14)	3957(7)	102(4)
O(2)	4035(24)	178(52)	5000	109(14)
O(3)	3116(45)	2196(35)	5000	156(20)
O(4)	3885(24)	1170(65)	5000	134(20)
O(5)	2308(35)	1865(35)	5000	186(23)
		PtCl(25 °C)		
Pt(1)	0	0	2500	24(1)
N(1)	1000(4)	1589(6)	2481(4)	37(1)
C(1)	490(6)	2884(8)	2809(7)	49(3)
Cl(1)	0	0	356(4)	35(1)
Cl(2)	2977(2)	794(3)	5000	49(1)
O(1)	2632(6)	181(7)	3913(6)	81(3)
O(2)	4038(13)	335(23)	5000	64(7)
O(3)	2959(27)	2198(25)	5000	104(11)
O(4)	2142(22)	1958(28)	5000	125(13)
O(5)	3786(20)	1649(40)	5000	114(13)
		PtBr(25 °C)		
Pt	0	0	0	16(1)
Br	146(1)	2264(3)	−33(1)	27(1)
Cl(1)	3602(3)	2500	7205(3)	32(1)
Cl(2)	6838(3)	2500	2520(3)	28(1)
N(1)	51(8)	45(4)	2413(7)	24(2)
N(2)	2722(8)	−50(4)	1083(8)	25(2)
C(1)	1856(10)	−344(7)	3521(9)	32(3)
C(2)	3192(9)	245(7)	2870(9)	31(3)
O(21)	6365(8)	1419(5)	1618(7)	48(3)
O(22)	5941(8)	2500	3809(9)	41(3)
O(23)	8743(8)	2500	3447(9)	47(3)
O(31)	3158(9)	1431(6)	7888(9)	67(3)
O(32)	5488(9)	2500	7530(10)	50(3)
O(33)	2733(12)	2500	5480(10)	87(5)
		PtCl(−20 °C)		
Pt	0	0	0	18(1)
Cl(1)	108(5)	2130(4)	−53(5)	28(1)
Cl(2)	3630(4)	2500	7253(4)	29(1)
Cl(3)	6856(4)	2500	2631(4)	24(1)
N(1)	27(10)	59(6)	2425(10)	25(3)
N(2)	2705(11)	−34(5)	1060(10)	25(3)
C(1)	1844(12)	−326(8)	3523(13)	27(3)
C(2)	3188(11)	269(8)	2873(11)	26(3)
O(21)	6378(9)	1407(7)	1616(9)	45(3)
O(22)	6002(11)	2500	3865(13)	36(4)
O(23)	8767(10)	2500	3434(13)	43(4)
O(31)	3162(9)	1416(8)	7959(11)	59(3)
O(32)	5533(10)	2500	7585(14)	43(4)
O(33)	2689(15)	2500	5460(15)	71(5)

[a] Equivalent isotropic U defined as one-third of the trace of the orthogonalized U_{ij} tensor.

coordinates and isotropic thermal parameters are listed in Table II for the PtBr(40 °C), PtCl(25 °C), PtCl(−20 °C), and PtBr(25 °C) structures. Atomic coordinates and isotropic thermal parameters for the low-temperature structures were deposited as supplementary material.

***Ibam* Structures.** In these systems the Pt atom sits on a site of 222 symmetry. 1,2-Diaminoethane ligands compose the equatorial plane. The unique Pt–N distance is 2.050(5) Å in PtCl(25 °C) and 2.063(6) Å in PtBr(40 °C). The ethylenediamine groups assume the gauche conformation. The axial sites of the Pt atom are occupied by bridging halogen atoms (Figure 1). The bridging halogen atoms do not sit halfway between the platinum atoms, where there is an inversion center, but rather just off of this symmetry element. This yields two halogen atoms in the bridging region; each halogen atom is at half-occupancy, and the doublet is the result of an average structure of alternately

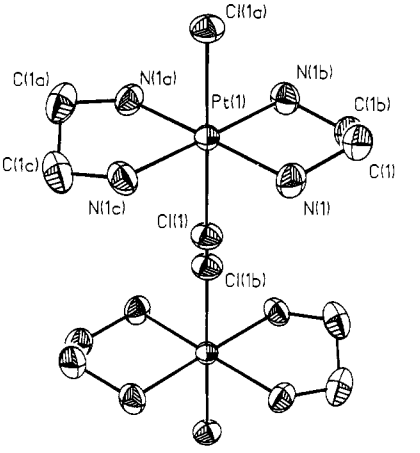

Figure 1. Diagram of a portion of the PtCl orthorhombic phase showing thermal ellipsoids. The presence of two Cl atoms in the bridging region is the result of an average structure resulting from chain stacking faults in the crystal (Figure 2).

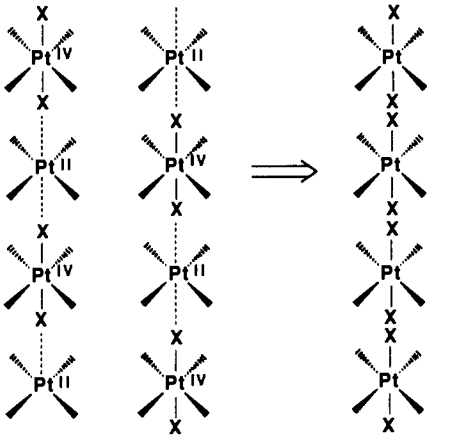

Figure 2. Diagram of PtX chains showing disorder. The observed structure of the right-hand side of the arrow is an average of the two mismatched chains in the left-hand side of the arrow.

stacked PtX chains (Figure 2). Each chain consists of alternating Pt–X bond distances, as may be observed in one of the chains of the left-hand side of Figure 2. In the Cl analog the short Pt–Cl distance is 2.327(4) Å and the long Pt···Cl distance is 3.101(4) Å. In the Br analog these distances are 2.488(2) and 3.009(2) Å, respectively. The PtX chains in these structures are perfectly linear (by symmetry), with Pt–X–Pt angles of 180(0)°.

The perchlorate ions sit on mirror planes in these systems. Two of the oxygens and the chlorine sit on the mirror plane, with the remaining oxygens above and below the mirror plane. The perchlorate ions are located between the PtX chains, serving to isolate them from one another. However, the chains are weakly linked via a hydrogen-bonding network (Figure 3). The oxygens in the perchlorate ions hydrogen bond to the NH_2 hydrogens in the 1,2-diaminoethane ligand. These hydrogen bonds are listed in Table IVa. The H···O distances in PtCl(25 °C) range from 2.410 to 2.472 Å (av = 2.441), with the range being 2.399–2.441 (av = 2.420) for PtBr(40 °C). This implies a slightly stronger hydrogen-bonding network in the Br analog, a point that will be developed below.

***P*2$_1$/*m* Structures.** In these structures the Pt atoms occupy centers of inversion. The equatorial plane contains two 1,2-diaminoethane ligands, both in the gauche conformation. The unique Pt–N distances are 2.050(8) and 2.055(9) Å for PtCl(−20 °C) and 2.046(7) and 2.056(6) Å for PtBr(25 °C). The axial sites are composed of bridging halide atoms. These halogen atoms sit just off of a mirror plane, resulting in two bridging halides in the averaged structure (Figure 2). One individual chain is shown in Figure 4 for the PtCl(−20 °C) monoclinic structure. In the

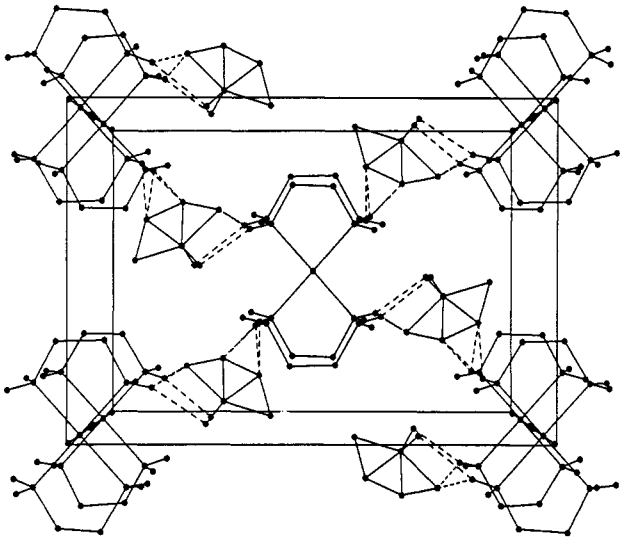

Figure 3. Unit cell packing diagram of the orthorhombic phase of PtCl. The projection is along the chain axis (*c*-axis). Hydrogen bonding is shown with dashed lines.

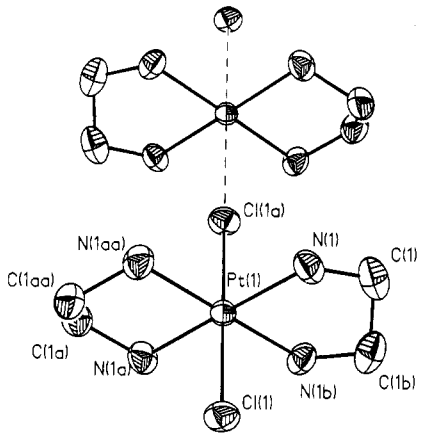

Figure 4. Diagram of a portion of the PtCl monoclinic phase showing thermal ellipsoids.

Cl analog the short Pt–Cl distance is 2.319(5) Å and the long Pt···Cl distance is 3.122(5) Å. The corresponding PtBr distances are 2.484(3) and 3.001(3) Å, respectively. The PtX chains in these structures are buckled; the Pt–X···Pt angle is 175.3(2)° for the Cl analog and 174.6(1)° for the Br analog. This buckling may be observed in Figure 4.

The perchlorate ions sit on mirror planes in these systems. Two of the oxygens and the chlorine sit on the mirror plane, with the remaining oxygens above and below the mirror plane. In addition, the oxygens on the mirror plane are disordered, occupying $^1/_4$ occupancy sites. The perchlorate ions serve to link the PtX chains together via a weak hydrogen-bonding network (Figure 5). The oxygens in the perchlorate ions hydrogen bond to the NH_2 hydrogens in the 1,2-diaminoethane ligand. These hydrogen bonds are listed in Table IVb. The H···O distances in PtCl(−20 °C) range from 2.069 to 2.443 Å (av = 2.276), with the range being 2.088–2.396 (av = 2.261) for PtBr(25 °C). As in the orthorhombic structures, the PtBr system has a slightly stronger hydrogen-bonding network.

The very low temperature monoclinic phases of PtBr and PtCl [PtBr(−93 °C) and PtCl(−20 °C)] are isostructural with the corresponding high-temperature monoclinic phases [PtBr(25 °C) and PtCl(−20 °C)]. In the chloride analog the Pt–Cl, Pt···Cl, and ρ remain constant to within experimental error upon cooling from −20 to −70 °C. In the bromide analog a decrease upon cooling from 25 to −93 °C is noted in the Pt···Br and Pt–Br bond distances. The strength of the CDW, as measured by ρ, weakens from 0.828(1) at 25 °C to 0.832(1) at −93 °C. The buckling also

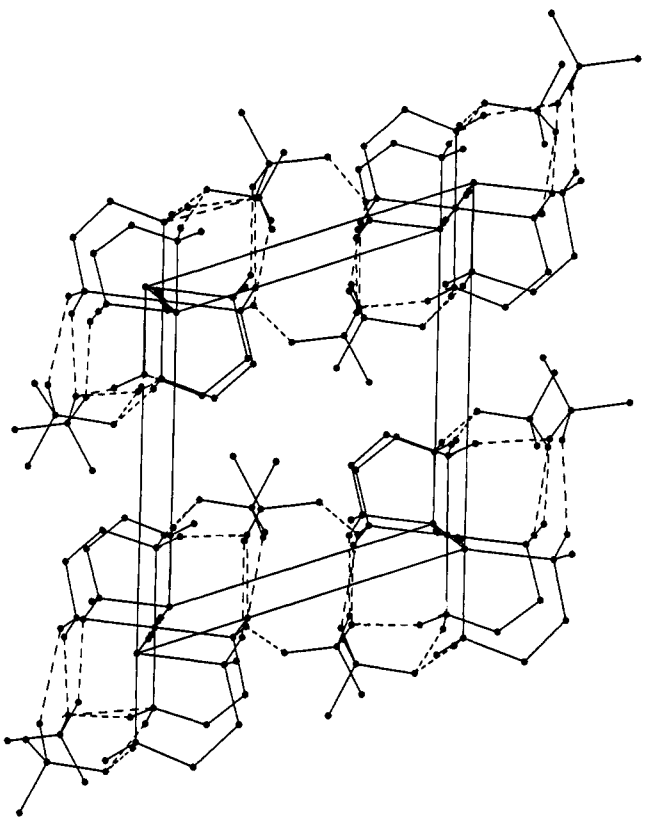

Figure 5. Unit cell packing diagram of the monoclinic phase of PtCl. The projection is along the chain axis (*b*-axis). Hydrogen bonding is shown with dashed lines.

increases upon cooling in the bromide salt; a decrease from 174.6(1) to 174.1(1)° occurs upon cooling from 25 to −93 °c, respectively. The buckling angle remains constant, within experimental error, upon cooling from −20 to −70 °C in PtCl.

Raman Results

The Raman spectra of PtX materials are dominated by the X–Pt(IV)–X symmetric stretch mode (ν_1), which because it is coupled to the Peierls distortion, displays dramatic resonant enhancement when the exciting light is close in energy to the metal–metal intervalence charge-transfer (IVCT) absorption band.[1] Here we find a direct correlation between the frequency of ν_1 in a given material and the CDW strength as measured by ρ, with a stronger CDW corresponding to a higher ν_1 frequency. This correlation has also been noted in high-pressure studies in which ν_1 tracks the pressure variation of the CDW strength as measured by the IVCT energy[19] and in studies for which the CDW strength of chloride-bridged Pt chains is varied by changing the ligand–counterion system.[20a,b]

PtCl. The temperature dependence of ν_1 in PtCl is shown in Figure 6a. The frequency of the ν_1 Raman peak, obtained by curve-fitting of the ν_1 peak region, for isotopically pure $Pt^{35}Cl$ probed using 841-nm excitation is shown by solid triangles in Figure 6a. Solid squares and open circles represent the frequency of the dominant central peak of the isotopic fine structure[21] of PtCl with natural Cl isotopic abundance (75% ^{35}Cl, 25% ^{37}Cl),

(19) Donohoe, R. J.; Love, S. P.; Garcia, M. A. Y.; Swanson, B. I. In *Frontiers of High Pressure Research*; Hochheimer, H. D., Etters, R. D., Eds.; Plenum: New York, 1991.
(20) (a) Scott, B.; Donohoe, R. J.; Love, S. P.; Johnson, S. R.; Wilkerson, M. P.; Swanson, B. I. *Inorg. Chem.*, submitted for publication. (b) Scott, B.; Donohoe, R. J.; Love, S. P.; Johnson, S. R.; Wilkerson, M. P.; Swanson, B. I. *Synth. Met.*, in press. (c) Larsen, K. P.; Toftlund, H. *Acta Chem. Scand.* **1977**, *A31*, 182. (d) Clark, R. J. H. *Ann. N.Y. Acad. Sci.* **1978**, *313*, 672.
(21) Love, S. P.; Worl, L. A.; Donohoe, R. J.; Huckett, S. C.; Swanson, B. I. *Phys. Rev. B* **1992**, *46*, 813.

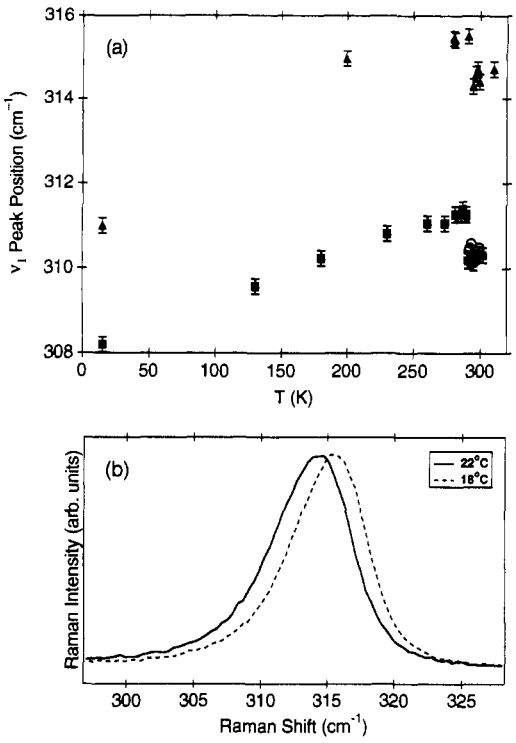

Figure 6. (a) Position of the fundamental Cl–Pt^{IV}–Cl symmetric stretch (ν_1) Raman mode of PtCl as a function of temperature. Solid triangles: isotopically pure Pt^{35}Cl grown at 10 °C, 841-nm excitation. Solid squares: PtCl with natural Cl isotopic abundance, grown at 40 °C, 841-nm excitation. Open circles: PtCl with natural Cl isotopic abundance, grown at 40 °C, 514.5-nm excitation. For the natural isotopic abundance sample, the position of the strong central feature of the isotopic fine structure is plotted. (b) Raman spectra, excited at 841 nm, of isotopically pure Pt^{35}Cl at 18 and 22 °C, showing the shift of ν_1 at the phase transition.

probed using 841- and 514.5-nm excitation, respectively. Both examples of natural-abundance PtCl shown in Figure 6a were grown in the orthorhombic phase at 40 °C and maintained above 20 °C until Raman measurements were performed. The data shown by the solid squares and open circles in Figure 6a represent cooling the sample through the transition. The Pt^{35}Cl sample was grown in the monoclinic phase at 10 °C and carefully maintained below the phase transition temperature, so that the solid triangles in Figure 6 represent warming through the transition.

In all cases the same behavior is observed: Below the phase transition, ν_1 increases monotonically with increasing temperature, in a roughly linear fashion, from 311.0 cm^{-1} for Pt^{35}Cl and 308.2 cm^{-1} for natural abundance PtCl at 15 K to 315.5 ± 0.2 cm^{-1} for Pt^{35}Cl and 311.3 ± 0.2 cm^{-1} for natural PtCl at 19 °C, immediately below the transition. A discontinuous decrease in ν_1 by 1 cm^{-1} occurs upon warming through the phase transition, with values of 314.5 and 310.3 ± 0.2 cm^{-1} observed immediately above the transition temperature for Pt^{35}Cl and natural-abundance PtCl, respectively. Above the transition temperature, the general increase of ν_1 with increasing temperature continues. Subsequent measurements with the same crystals demonstrate that the behavior shown in Figure 6 is reversible, at least for the first few cycles through the phase transition. Shown in Figure 6b is the Raman spectrum of Pt^{35}Cl at temperatures immediately above and below the transition temperature, illustrating the size of the shift relative to the natural line width at this temperature. The instrumental resolution, roughly 0.4 cm^{-1}, is much smaller than the natural line width at these temperatures. Since we use a CCD array detector, no mechanical movement of the spectrometer occurs between measurements, thus eliminating the largest possible source of error in comparing the ν_1 frequencies for different temperatures; the instrumental precision for such frequency comparisons is better than 0.2 cm^{-1}, much smaller

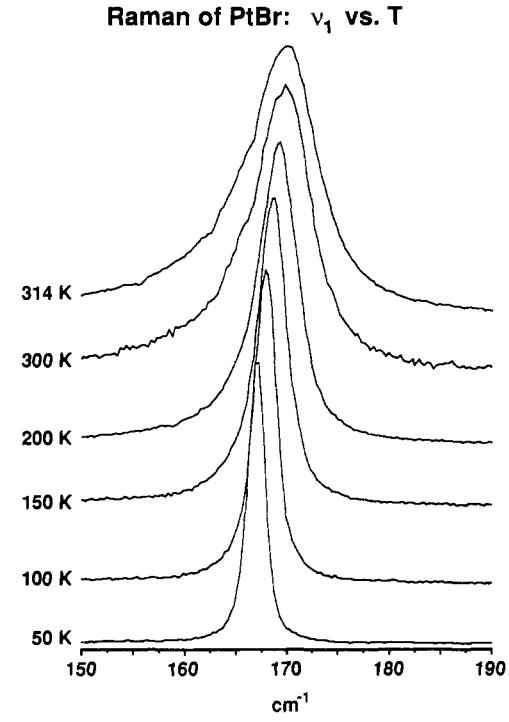

Figure 7. Raman spectrum of PtBr as a function of temperature, showing the evolution of the Br–Pt^{IV}–Br symmetric stretch (ν_1) mode. Spectra were obtained using 980-nm excitation.

than the observed ν_1 shift at the phase transition. Indeed, since PtCl ν_1 Raman scattering is very strong, it is possible to monitor the Raman spectrum essentially in real time (CCD integration times of 1 or 2 s) and observe directly the abrupt shift in the ν_1 frequency as the sample temperature is gradually scanned through the transition temperature.

PtBr. Figure 7 shows the Raman spectrum of PtBr in the ν_1 region as a function of temperature, obtained using 980-nm excitation. As with the PtCl, PtBr's ν_1 frequency increases monotonically with increasing temperature below the phase transition. But unlike PtCl, no measurable frequency drop at the phase transition is observed.

Discussion

The greatest differences in the orthorhombic, *Ibam* structures and the monoclinic, $P2_1/m$ structures lie in the perchlorate ions and their corresponding hydrogen-bonding network. The perchlorate ions are fully ordered in the monoclinic phases. The perchlorate ions in the orthorhombic phases are disordered and have much larger O thermal parameters than in the corresponding monoclinic phases (Table II). This increased thermal motion is responsible for a weakening of the hydrogen-bonding network in going from the monoclinic to orthorhombic phases; O···H bond distances range 2.069–2.443 Å in the PtCl monoclinic phase versus 2.410–2.472 Å in the PtCl orthorhombic phase. A similar weakening is noted in the PtBr material (2.088–2.396 Å versus 2.399–2.441 Å in going from monoclinic to orthorhombic, respectively). This change in the hydrogen-bonding network, brought on by increased perchlorate thermal motion, is responsible for the different packing arrangements in the monoclinic and orthorhombic structures (Figures 3 and 5). In the monoclinic structure the hydrogen bonding serves to link the chains together along the *a*-axis (Figure 5). In the orthorhombic structure a three-dimensional network of hydrogen bonds is realized (Figure 3). In both phases hydrogen bonding also links adjacent en ligands within a chain. Small changes in the positions of the perchlorate ions are also noted between the phases.

A comparison of the hydrogen bonding between the PtCl structures and the PtBr structures is also informative. The

Table III. Selected Bond Angles (deg) and Distances (Å) for the Title Compounds

cryst(T/°C)	Pt(II)–X	Pt(IV)–X	Pt(IV)–X/ Pt(II)–X
PtBr(40)	3.009(2)	2.488(2)	0.827(1)
PtBr(25)	3.001(3)	2.484(3)	0.828(1)
PtBr(–93)	2.978(3)	2.479(2)	0.832(1)
PtCl(25)	3.101(4)	2.327(4)	0.750(1)
PtCl(–20)	3.122(5)	2.319(5)	0.743(1)
PtCl(–70)	3.119(4)	2.322(4)	0.744(2)

cryst(T/°C)	Pt–N	N–C	C–C
PtBr(40)	2.063(6)	1.500(1)	1.463(20)
PtBr(25)	2.046(7), 2.056(6)	1.480(10), 1.497(9)	1.498(12)
PtBr(–93)	2.045(6), 2.049(6)	1.488(7), 1.484(9)	1.504(10)
PtCl(25)	2.050(5)	1.474(9)	1.492(17)
PtCl(–20)	2.050(8), 2.055(9)	1.506(11), 1.499(12)	1.502(15)
PtCl(–70)	2.045(8), 2.053(6)	1.490(9), 1.496(8)	1.517(10)

cryst(T/°C)	Pt–N–C	N–C–C	Pt–X–Pt
PtBr(40)	108.9(5)	109.9(6)	180(0)
PtBr(25)	108.9(5), 109.1(5)	107.1(6), 108.6(5)	174.6(1)
PtBr(–93)	108.4(4), 109.2(5)	107.5(5), 107.8(5)	174.1(1)
PtCl(25)	108.74	108.1(5)	180(0)
PtCl(–20)	107.9(8), 109.7(5)	107.4(8), 108.3(9)	175.3(2)
Pt–Cl(–70)	108.3(5), 109.9(5)	106.9(5)	175.0(1)

Table IV. Hydrogen Bond Distances (Å) in the Title Compounds

bond	PtCl	PtBr	bond	PtCl	PtBr
		(a) Orthorhombic Phases[a]			
N1–O3	3.260	3.247	O3···H1	2.410	2.399
N1–O5	3.200	3.263	O5···H2	2.472	2.441
N1–O3^{i}	3.260	3.247	O3^{i}···H1	2.410	2.399
N1–O5^{i}	3.200	3.263	O5^{i}···H2	2.572	2.441
		(b) Monoclinic Phases[b]			
N1–O23	3.057	3.080	O23···H2	2.179	2.202
N1–O31	2.934	2.950	O31···H	2.069	2.088
N1–O23^{i}	3.057	3.080	O23^{i}···H2	2.179	2.202
N2–O21	3.002	2.958	O21···H4	2.443	2.396
N2–O32	3.073	3.043	O32···H3	2.300	2.274
N2–O32^{ii}	3.073	3.043	O32^{i}···H4	2.300	2.274
N2–O31	3.192	3.188	O31···H3	2.401	2.390

[a] Symmetry code: i = $^1/_2 - x$, $^1/_2 - y$, $^1/_2 - z$. [b] Symmetry codes: $i = x - 1$, $^1/_2 - y$, z; ii = $1 - x$, $-^1/_2 + y$, $1 - z$.

hydrogen-bonding network in the PtCl structures is weaker than in the corresponding PtBr structures (vide supra and Table IV). This is in agreement with the lower phase transition temperature of the PtCl material (19.8 °C for PtCl and 28.7 °C for PtBr).

The change in crystal packing between the orthorhombic and monoclinic phases also has consequences for the PtX chain geometries. In the orthorhombic phases the Pt–X–Pt angles are 180°, while in the monoclinic structures these angles are substantially less than 180° (Table III). This buckling of the Pt–X–Pt angle increases with decreasing temperature and is probably the result of the contracting Pt–Pt distance straining the chain geometry. As observed in Figure 1, there are two positions for the bridging halides, each having $^1/_2$ site occupancy. These two sites correspond to stacking faults between chains in the crystal (Figure 2). These stacking faults are responsible for the diffuse sheets observed in the chain axis axial photographs. Attempts to induce chain to chain order by growing crystals in a pressure cell have not been successful.

The phase dependence of the CDW in these systems is significantly different in the PtCl and PtBr materials. In the bromide case the strength of the CDW (proportional to ρ = Pt-(IV)–X/Pt(II)···X) does not change through the phase transition (Table III). The long and short Pt–Br distances remain essentially constant. This is born out in the resonance Raman spectra (Figure 7), which also shows no change through the phase transition. In contrast, the PtCl materials show a significant change in CDW strength, going from ρ = 0.743(1) at –20 °C to 0.750(1) at 25 °C. This jump in ρ is concomitant with a decrease in the long Pt–Cl distance and a roughly constant short Pt–Cl distance. This result is also substantiated in the Raman spectra (Figure 6), where a 1-cm^{-1} jump, corresponding to a CDW softening, is observed. It is true that the temperature difference between the measured monoclinic and orthorhombic structures is different for PtCl (ΔT = 45°) and PtBr (ΔT = 15°). However, when the structural results are combined with the Raman results, there is strong evidence for a difference in behavior in the CDW strength of these two materials at the phase transition. This difference is probably the result of differences in hydrogen bonding between the PtCl and PtBr structures. In the monoclinic phases of both materials the CDW weakens as the temperature is lowered, as indicated by both the Raman and X-ray results (Figures 6 and 7 and Table III).

The previous inconsistencies in the PtBr structure literature may be explained by invoking Cl impurities. In particular, the orthorhombic structure reported in space group *Ic2a* is of interest. The *b*-axis (chain axis) lattice constant for this crystal was reported as 10.914(8) Å. In comparison with other PtBr structures, this distance is significantly shorter and implies a large amount of Cl doping [10.994(2) Å for the pure orthorhombic phase of PtBr(40 °C) determined in this work]. Raman spectroscopy carried out in this laboratory show that in such systems a significant amount of Br–Pt–Cl type sites exists.[10] A large number of such sites could skew the diffraction statistics, thus making the acentric space group *Ic2a* favored over the centric *Icma* of the pure PtBr. It was shown in a recent work[12] that the X-ray-induced phase transitions observed in these crystals correspond to heating of the crystal in the X-ray beam; the Cl impurities lower the phase transition temperature to around 26 °C. Finally, it is not completely understood how the space group *I*222 could be assigned to the orthorhombic PtBr structure. One explanation is that a doped crystal with a phase transition very near room temperature was used and that phase inhomogeneities somehow altered the systematic absences.

The lattice and Pt–Cl bond distances reported in this work differ significantly from those reported by Kida et al. in an earlier work.[13] The largest discrepancy is in the chain lattice constant, where Kida reports a value of 10.807(2) Å [this work reports 10.855(4) Å for PtCl(25 °C)]. This value led the previous researchers to short and long Pt–Cl distances of 2.318(7) and 3.085(7) Å, respectively. Our structure determination resulted in short and long distances of 2.327(4) and 3.101(4) Å, respectively. Kida also reported lattice constants perpendicular to the chain lattice constant that are also quite short as compared to this work; 13.525(2) and 9.643(1) Å versus 13.594(4) and 9.657(5) Å. One possible explanation for the smaller unit cell reported by Kida is a large amount of Cl^- impurities in the perchlorate counterion sites. This would shrink the size of the unit cell. Evidence for such impurities has recently been discovered.[20a]

Weakening of the CDW strength, in PtBr and PtCl, with decreasing temperature is strongly supported by resonance Raman spectroscopy and is consistent with the X-ray diffraction results. Figures 6 and 7 show that the symmetric X–Pt–X stretching frequency (ν_1) decreases with decreasing temperature. The *b*-axis lattice constants indicate a shortening of the Pt–Pt distance with decreasing temperature within the monoclinic phases of PtCl and PtBr. The X-ray results also show that the short Pt(IV)–Br bond in PtBr remains essentially constant, while the long Pt-(II)–Br bond decreases in length, thus leading to a softening of the CDW strength with decreasing temperature. A very similar trend is seen in the literature as well. For example, the compounds $[Pt(cxhn)_2Cl_2][Pt(chxn)_2]Cl_4$, $[Pt(en)_2Cl_2][Pt(en)_2](ClO_4)_4$, and $[Pt(cxhn)_2Cl_2][Pt(chxn)_2]Cl_4$ have CDW strengths of 0.820, 0.750, and 0.681, respectively. The ν_1 frequencies of these salts are 280, 311, and 342 cm^{-1}, respectively. Therefore, there is a direct relationship between ν_1 and the CDW strength; softer

CDW's result in lower ν_1 frequencies.[20a] The PtBr data show this trend: PtBr(25 °C) has $\rho = 0.828(1)$ and $\nu_1 = 167$ cm^{-1}, while PtBr(−93 °C) has $\rho = 0.832(1)$ and $\nu_1 = 165$ cm^{-1}. It is true that this effect is not obvious from the PtCl structural results ($\rho = 0.743(1)$ at 20 °C and $\rho = 0.744(2)$ at −70 °C), but this is due to a smaller temperature range for the diffraction experiment. However, Raman results strongly indicate softening of the CDW strength with decreasing temperature for PtCl in the monoclinic phase.

Although the CDW strength weakens upon cooling in PtCl and PtBr, it never becomes fully quenched ($\rho = 1$), and these systems remain strong CDW systems throughout the temperature range of the experiment. Larger control over the CDW strength may be achieved through the application of hydrostatic pressure. It has been shown that 3 GPa of pressure produces a negative shift in ν_1 of −16 cm^{-1} in both PtCl and PtBr.[19] This shift corresponds to a substantial weakening of the CDW strength, and X-ray structure studies as a function of pressure are currently underway to measure just how large this effect is. The largest control over CDW strength, however, is achieved chemically (vide supra). We have recently shown that in a series of chloride-bridged Pt chains that the CDW strength may be tuned from $\rho = 0.681$ to 0.820 by simply changing the counterion/ligand system.[20a] The same study also shows a similar trend for the bromide bridged series; ρ may be tuned from 0.741 to 0.866. Large changes in the IVCT energy and ν_1 are also observed as the result of this chemical tuning. There is also a case in the literature where an MX system has been taken to a $\rho = 1$, M(III)–X–M(III) valence formalism; $[Ni(chxn)_2Br_2][Ni(chxn)_2]Br_4$, where chxn = 1,2-diaminocyclohexane, is a spin-density-wave system.[22] The high tunability of MX systems allows a variety of materials with different optical and transport properties to be accessed, making this class of materials a very interesting one to study the consequences of advanced materials design.

(22) Toriumi, K.; Yoshiki, W.; Mitani, T.; Bandow, S. *J. Am. Chem. Soc.* **1989**, *111*, 2341.

Conclusions

The crystal and molecular structures of the pure phases of PtCl and PtBr were determined. The ambiguities in previous structural reports on the PtBr materials were discussed in light of Cl impurities. The monoclinic phase of pure PtCl was determined for the first time and was found to be isostructural to the pure monoclinic PtBr phase. The structure determination of the orthorhombic phase of PtCl agreed with a previous study but was found to have a significantly larger unit cell, pointing to counterion impurities in the previously determined crystal structure. The temperature dependence of the phases of the PtX materials is manifested in crystal packing and PtX chain geometries, which are in turn are linked to changes in hydrogen bonding initiated by increased thermal motion in the perchlorate counterions. Both PtCl and PtBr show a softening of the CDW upon cooling. The structural results on these pure materials will aid studies on mixed-halide PtX systems, which are currently under investigation.

Acknowledgment. This work was supported by the Office of Basic Energy Sciences, Division of Materials Science of the DOE, and the Center for Materials Science at LANL.

Supplementary Material Available: Tables giving crystal data and details of the structure determination, atom coordinates, bond lengths, bond angles, anisotropic thermal parameters, and hydrogen atom locations (36 pages). Ordering information is given on any current masthead page.